©2005 The Visualization Society of Japan and Ohmsha, Ltd.
Journal of Visualization, Vol. 8, No. 2 (2005)177-185

Visualization and Characterization of Small-Scale Spanwise Vortices in Turbulent Channel Flow

Christensen, K. T.*[1] and Wu, Y.*[2]

*1 Department of Theoretical and Applied Mechanics, University of Illinois at Urbana-Champaign, Urbana, IL, 61801, USA. E-mail: ktc@uiuc.edu
*2 Department of Theoretical and Applied Mechanics, University of Illinois at Urbana-Champaign, Urbana, IL, 61801, USA.

Received 11 October 2004
Revised 18 November 2004

Abstract : High-resolution particle-image velocimetry (PIV) measurements are made in the streamwise–wall-normal plane of turbulent channel flow at $Re_\tau = 566$, 1184 and 1759, facilitating documentation of the population trends and core diameters of small-scale spanwise vortices. Swirling strength, an unambiguous vortex-identification criterion and hence a local marker of rotation, is used to extract small-scale spanwise vortex cores from the instantaneous velocity fields. Once the small-scale vortices are properly extracted from the PIV realizations, their characteristics are studied in detail. The present results indicate that the very-near-wall region ($y < 0.1h$) is densely populated by spanwise vortices with clockwise (negative) rotation. This behavior supports the notion that hairpin-like vortices are generated very close to the wall and grow into the outer layer as they advect downstream. In contrast, counterclockwise (positive) spanwise vortices are scarce in the very-near-wall region, but their presence steadily increases within the logarithmic layer presumably due to a localized generation mechanism. The average core diameter of negative spanwise vortices is found to be larger than the average diameter of positive vortices, with few positive vortices having core diameters exceeding $80y_*$.

Keywords : Turbulence structure, Vortex visualization, Wall turbulence, PIV.

1. Introduction

There is broad evidence that a vortical structure qualitatively similar to the “horseshoe vortex” first proposed by Theodorsen (1952) does exist in wall turbulence. Both the inner and outer layers of wall turbulence contain inclined structures which are associated with ejections and sweeps (Head and Bandyopadhyay, 1981; Smith, 1984; among others). Head and Bandyopadhyay (1981), in particular, visualized ramp-like patterns at the outer-most edge of the boundary layer, and proposed this to be the imprint of groups of hairpin vortices inclined away from the wall at a shallow angle. More recently, Adrian et al. (2000b) found that hairpin-like vortices actually align coherently in the streamwise direction, creating larger-scale coherent motions (hairpin vortex packets) that occur throughout the outer region in a hierarchy of scales. The heads of these vortices appear as swirling patterns with clockwise rotation in the streamwise–wall-normal plane (negative spanwise vorticity) which is consistent with the character of the mean shear.Christensen and Adrian (2001) used conditional averaging techniques to show that this vortex organization is a dominant, coherent feature of the flow that contributes significantly to the multi-point statistics. This conclusion is further supported by the work of Marusic (2001), who determined that the long streamwise tail of the streamwise velocity correlation in the log layer is attributable to outer-layer vortex organization

Table 1. Summary of flow parameters and resolution of PIV measurements.

Re_τ	ρ (kg/m^3)	ν (m^2/s)	τ_w (Pa)	u_* (m/s)	y_* (μm)	Δx (μm)	Δy (μm)	No. of vectors per realization
566	1.000	1.80×10^{-5}	0.17	0.41	44.1	410 ($9.3y_*$)	410($9.3y_*$)	4,758
1184	0.999	1.81×10^{-5}	0.73	0.85	21.2	205($9.7y_*$)	205($9.7y_*$)	19,468
1759	0.997	1.81×10^{-5}	1.62	1.27	14.2	128($9.0y_*$)	128($9.0y_*$)	46,930

Finally, the work of Kim and Adrian (1999) indicates that this outer-layer vortex organization may extend to very-large-scale motions having streamwise extents of several outer length scales.

The spatial characteristics of large-scale outer-layer vortex organization have recently been documented by Christensen et al. (2004) and Wu (2004). The average length of the packets was found to grow with Reynolds number, when scaled by the outer length scale, and the vortices within a given packet traveled, on average, at the local mean velocity. Further, the streamwise spacing between vortices in a packet was found to grow with wall-normal position but displayed some Reynolds-number similarity when scaled by the viscous (inner) length scale. This latter observation, when coupled with the finding that the length of these packets increases with Reynolds number, indicates that the number of vortices per packet might also increase with Reynolds number.

The goal of the present effort is to study the character of *small-scale* spanwise vortices in wall turbulence, particularly vortices with negative spanwise vorticity (heads of hairpin-like vortices) that are the building-blocks of larger-scale vortex packets. The presence of small-scale spanwise vortices with opposite rotation (positive spanwise vorticity) is also considered. A methodology for identifying and visualizing the small-scale structure embedded within the instantaneous high-resolution PIV fields is presented. Vortex population trends and core diameters are then assessed based upon the vortices extracted from the PIV ensembles.

2. Experiment

2.1 Flow Facility

All experiments discussed herein are performed in turbulent channel flow (see Wu (2004) for details). The flow facility is a closed circuit system, the working fluid is air, and it is driven by a five-horsepower cent-axial blower. Air passes through a flow-conditioning section which includes honeycomb, a series of screens, and a smooth contraction that guides the flow into the 50 mm × 600 mm ($2h$ × width, where h is the half-height of the channel) channel cross-section. The channel development length is 6.3 m long ($252h$), including a 1.3 m test section. The test section includes optical access from all directions and static pressure taps are mounted along the length of the channel allowing documentation of the streamwise pressure distribution. In two-dimensional turbulent channel flow, knowledge of dP/dx allows direct determination of the wall shear stress, τ_w, via integration of the mean streamwise momentum equation. Once τ_w and the fluid properties are known, the friction velocity, $u_* = (\tau_w/\rho)^{1/2}$, and the viscous length scale, $y_* = \nu/u_*$, can be assessed. All flow parameters are summarized in Table 1.

2.2 PIV Details

Particle-image velocimetry (PIV) is used to measure instantaneous two-dimensional velocity (u,v) fields in the streamwise–wall-normal $(x–y)$ plane along the channel's spanwise centerline at $Re_\tau \equiv u_*h/\nu$ = 566, 1184 and 1759. The air flow is seeded with nominally 1 μm olive oil droplets created by a Laskin nozzle and the $1.3h \times 1.0h$ (32.5 mm × 25.0 mm) field of view is illuminated with lightsheets formed from a pair of New Wave Research Gemini Nd:YAG lasers. Each laser pulse has a temporal width of 5 ns and 80 mJ of energy. The nominal thickness of the lightsheets in the test section is approximately 200 μm. The scattered light from the seed particles is imaged by a 1280 × 1024 pixel TSI PIVCAM 13-8 12-bit CCD camera with frame-straddle capabilities and a 105-mm focal length lens is used to image the particles with an f-number of 8. Two distinct images are acquired per vector field with a fixed time delay (Δt = 30 μs, 15 μs and 10 μs at Re_τ = 566, 1184 and 1759, respectively), facilitating two-frame cross-correlation analysis of the images. Two-thousand

statistically-independent image pairs are acquired at each Reynolds number.

The pairs of PIV images are interrogated using the *PIV Sleuth* software package (Christensen et al., 2000). The images are subdivided into square interrogation windows and a larger second window is selected to minimize bias errors associated with loss of image pairs. The images are analyzed with 50 % overlap to satisfy Nyquist's criterion and the second window is offset in the mean flow direction by the bulk displacement of the flow. Since our interest lies in studying the properties of small-scale vortices whose diameters are thought to scale with y_*, the size of the first interrogation window is chosen such that the vector grid spacing at each Re_τ is consistent when normalized by y_*. To meet this requirement, first interrogation windows with dimensions 32 × 32, 16 × 16, and 10 × 10 pixels are utilized at Re_τ = 566, 1184 and 1759, respectively, yielding a consistent inner grid spacing of approximately $9.0y_*$ at all three Re_τ (see Table 1). This inner-scale consistency implies that the grid spacing in physical (outer) units is largest at Re_τ = 566 (410 μm) and smallest at Re_τ = 1759 (128 μm) and, since the field of view is fixed in outer scales ($1.3h \times 1.0h$), the number of vectors per velocity realization is least at Re_τ = 566 (4,758 vectors) and greatest at Re_τ = 1759 (46,930 vectors). The PIV images at Re_τ = 566 and 1184 are analyzed using a standard single-pass interrogation. The Re_τ = 1759 ensemble, however, is analyzed using a multi-pass interrogation methodology in order to improve the quality of the result. Specifically, the Re_τ = 1759 images are first interrogated on a coarse grid (32 × 32 pixel first windows) with the second window offset by the bulk displacement of the flow. The same images are then re-interrogated on a finer grid (10 × 10 pixel first windows) and the second window is offset using locally-interpolated displacements from the coarse-grid interrogation.

The instantaneous vector fields at all three Re_τ are then validated using objective statistical methods to remove erroneous velocity vectors. Holes are filled either with alternative velocity choices determined *a priori* during interrogation or interpolated in regions where at least 50% of neighbors are present (The need for interpolation was minimal since, on average, over 99% of the velocity vectors in a given field were found to be valid *prior* to replacement and interpolation). Finally, each vector field is low-pass filtered with a Gaussian filter, whose width is smaller than the vector grid spacing, to remove high-frequency noise.

3. Vortex Identification

Identification of vortices in velocity fields, along with calculation of vortex statistics (i.e., size, strength, etc.), is normally accomplished by identifying isolated 'regions' of significant vorticity (vortex 'cores') (Jimenez et al., 1993). In simple flows with minimal shear, this task is relatively straightforward. However, in complex flow fields this is not the case. For example, wall-bounded turbulence is populated by strong shear layers that tend to mask turbulent eddies in vorticity maps. In such cases, the task of computing reliable vortex statistics is virtually impossible when using vorticity as a vortex identifier.

To alleviate these problems, several groups have proposed new methods of extracting underlying structure from velocity fields which involve analysis of the local velocity gradient tensor, ∇u_i, and its corresponding eigenvalues (Chong et al., 1990; Zhou et al., 1999; for example). In three dimensions, the local velocity gradient tensor will have one real eigenvalue (λ_r) and a pair of complex-conjugate eigenvalues ($\lambda_{cr} \pm i\lambda_{ci}$) when the discriminant of its characteristic equation is positive. In such instances, the particle trajectories about the eigenvector corresponding to λ_r exhibit a swirling spiral motion with λ_{ci}^{-1} representing the period required for a particle to swirl once about the λ_r-axis and λ_r representing the stretching incurred by the vortex (Chong et al., 1990). If the flow is pure shear flow, the particle orbits are infinitely-long ellipses and the orbit period is also infinite, corresponding to $\lambda_{ci} = 0$. Thus, $\lambda_{ci} > 0$ corresponds to shorter, more circular ellipses – *vortices*. In particular, Zhou et al. (1999) show that the strength of any local swirling motion is quantified by λ_{ci}, the *swirling strength* of the vortex. Vortex identification based on λ_{ci} is frame independent, meaning that *a priori* choice of a correct reference frame is not necessary. In addition, λ_{ci} does not reveal regions which have non-zero vorticity but are absent of any local swirling motion (i.e., shear layers). Since PIV fields are usually two-dimensional, the full local velocity gradient tensor cannot be formed. However, an equivalent two-dimensional form of this tensor can be computed in the plane in which the PIV data lies and ∇u_i will have either two real or a pair of complex-conjugate eigenvalues. Therefore, vortices are identified by regions of $\lambda_{ci} > 0$ (Adrian et al., 2000a).

4. Results

4.1 Vortex Extraction

Figure 1(a) presents an instantaneous velocity realization in the streamwise–wall-normal plane of turbulent channel flow at $Re_\tau = 566$. A constant advection velocity, U_c, is removed, revealing several vortices with clockwise and counterclockwise rotation advecting in the streamwise direction at U_c. In particular, when the chosen advection velocity matches an eddy's translational velocity, the vortex becomes recognizable as a roughly circular pattern of vectors representing closed streamlines, consistent with the definition of a vortex offered by Kline and Robinson (1989): "A vortex exists when instantaneous streamlines mapped onto a plane normal to the core exhibit a roughly circular or spiral pattern, when viewed in a reference frame moving with the center of the vortex core." Thus, vortices embedded within a turbulent flow can be revealed via Galilean decomposition by simply removing their advection velocities. However, since not all vortices move at the same speed, one must remove a broad range of advection velocities in order to reveal all embedded structure (Adrian et al., 2000a).

As noted in Section 3, more robust and less ambiguous methods for identifying vortices have been developed. Swirling strength is used in this effort since it is an unambiguous marker of rotation, is frame independent, and does not identify regions of intense shear, as is the case with vorticity. However, since the complex eigenvalues of ∇u_i occur in conjugate pairs, λ_{ci} alone cannot distinguish between vortices with clockwise rotation (negative vorticity) and vortices with counterclockwise rotation (positive vorticity). To overcome this deficiency, a modified swirling-strength parameter of the form

$$\Lambda_{ci}(x,y) \equiv \lambda_{ci}(x,y)\frac{\omega_z(x,y)}{|\omega_z(x,y)|}, \tag{1}$$

is proposed which represents both the presence of rotation and its direction. Therefore, Λ_{ci} yields clear distinction between vortex cores with counterclockwise and clockwise rotation. Figure 1(b) presents the instantaneous Λ_{ci} field computed from the velocity field shown in Fig. 1(a) (the phrase "swirling strength" will hereafter refer to Λ_{ci}). Swirling strength is noted at all locations where positive (red contours) and negative (blue contours) spanwise vortices are present in the single Galilean decomposition of the velocity field (Fig. 1(a)). However, non-zero Λ_{ci} is also noted at locations where closed streamlines are not clearly evident in the single Galilean decomposition. These regions of swirling strength represent vortices that are not moving at the advection velocity chosen for the Galilean decomposition. One can confirm this proposition directly by identifying peaks in $|\Lambda_{ci}|$ (the centers of the vortices) and extracting the instantaneous total velocity at each peak location (i.e., the instantaneous advection velocity of each individual vortex). These velocity vectors are overlaid onto the Λ_{ci} contours in Fig. 1(b) and clearly vary from vortex to vortex. Finally, to illustrate that each of these localized swirling-strength events corresponds to closed streamlines in the instantaneous velocity field, a local Galilean decomposition is performed in the immediate neighborhood of each $|\Lambda_{ci}|$ peak using the extracted instantaneous advection velocity at that peak (A vortex neighborhood is defined as the region about the center of a peak in $|\Lambda_{ci}|$ for which $|\Lambda_{ci}(x,y)| \geq \Lambda_{ci}^{rms}(y)$, where $\Lambda_{ci}^{rms}(y)$ is the root-mean-square value of Λ_{ci} at a given wall-normal location, y). This localized decomposition is presented in Fig. 1(c) and validates that all of the regions of non-zero Λ_{ci} in Fig. 1(b) are associated with closed-streamline patterns (vortices) in the instantaneous velocity.

The instantaneous example presented in Fig. 1 illustrates the effectiveness of Λ_{ci} in identifying and visualizing small-scale structure embedded within turbulent channel flow, particularly in terms of robustly defining a finite spatial neighborhood over which each vortex core resides. More importantly, Fig. 1 reveals that both positive and negative spanwise vortices can occur quite frequently in wall turbulence, although negative vortices appear to outnumber positive vortices by a factor of two or three in this particular example. In order to study the population trends and core diameters of these small-scale, spanwise vortex cores, instantaneous Λ_{ci} fields are computed for all instantaneous velocity realizations at all three Re_τ. Peaks in $|\Lambda_{ci}|$ are identified within each instantaneous velocity field, representing the centers of positive and negative spanwise vortex cores (The sign of Λ_{ci} at the peak location is used to distinguish between positive and negative vortices).

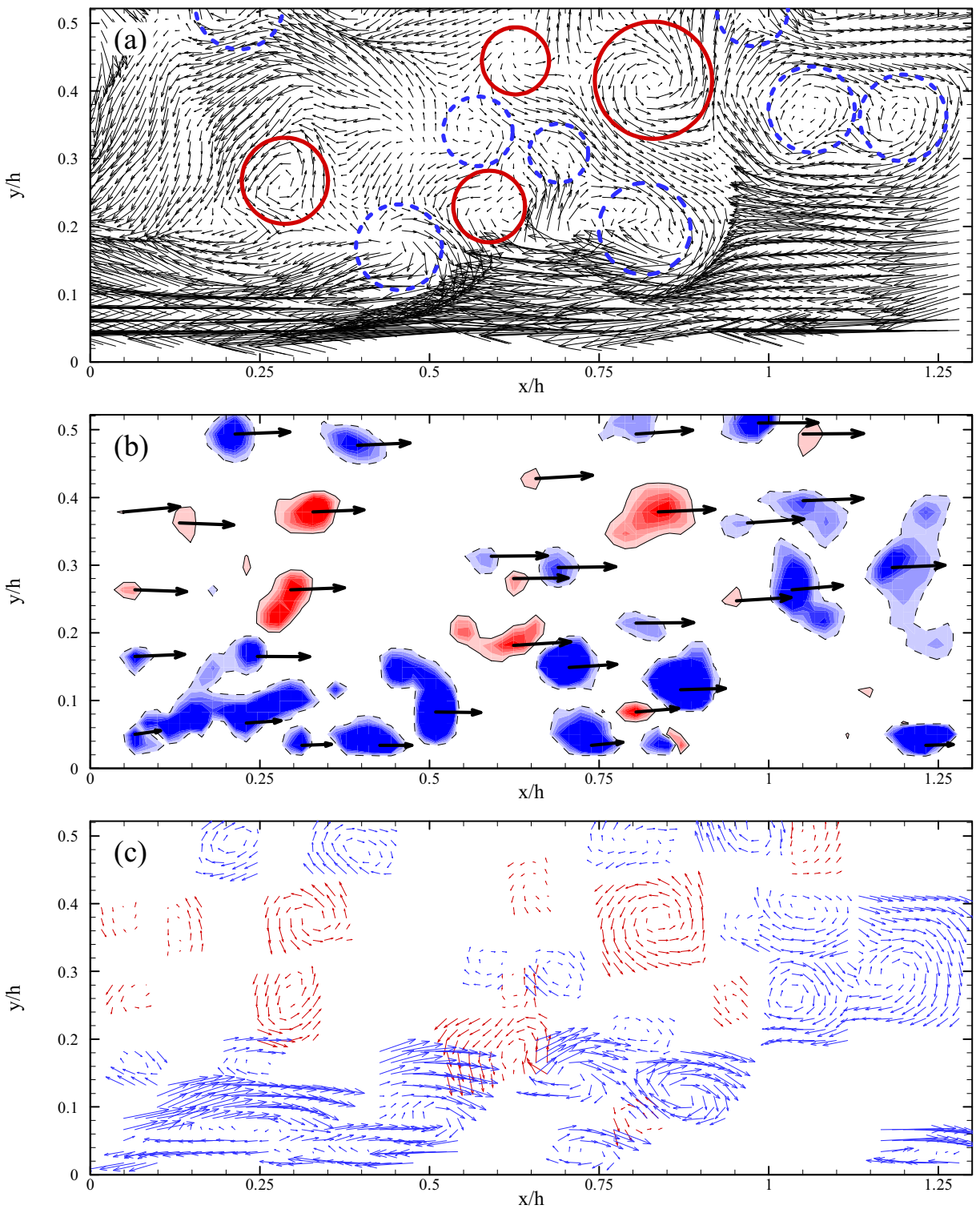

Fig. 1. Example of vortex identification in an instantaneous, two-dimensional PIV velocity field at Re_τ = 566. (a) Instantaneous velocity with a constant advection velocity removed (Galilean decomposition); (b) instantaneous swirling strength field associated with velocity field presented in (a); (c) velocity fields of vortex cores (local Galilean decomposition) extracted from (a). Vortex cores with positive vorticity are presented in red; vortex cores with negative vorticity are denoted by blue.

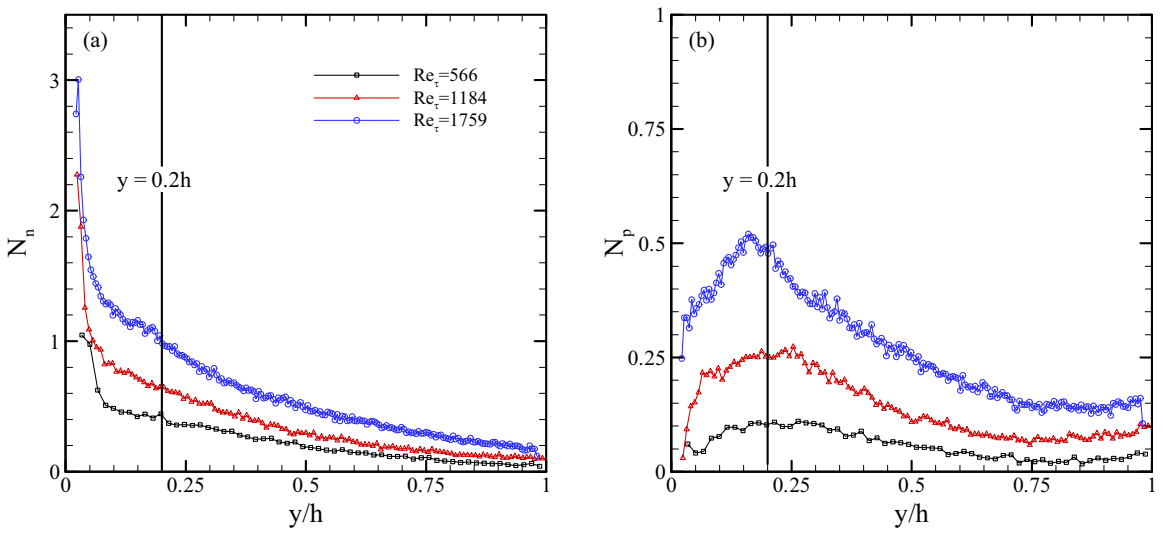

Fig. 2. Average number of (a) negative (N_n) and (b) positive (N_p) spanwise vortices per realization.

The spatial extent of each vortex is then extracted using the aforementioned neighborhood-identification methodology. However, if a vortex is found to have fewer than three grid points across its diameter that satisfy the neighborhood-identification requirement in either spatial direction, it is not considered due to insufficient spatial resolution. Therefore, since the vector grid spacing is roughly $9y_*$ at all three Re_τ, spanwise vortices with diameters less than approximately $18y_*$ are excluded from the present analysis. Once the vortices and their respective neighborhoods are identified, the population trends and core diameters of both negative and positive spanwise vortex cores can be explored.

4.2 Vortex Population Trends

Since the spatial location of each vortex center is unambiguously extracted from the Λ_{ci} fields, the population trends of both positive and negative spanwise vortices can be studied quite easily. Such trends in the inhomogeneous wall-normal direction (y) are crucial since they yield detailed information regarding the wall-normal regions where the majority of positive and negative spanwise vortices reside. In contrast, population trends of vortices in the streamwise direction (x) are not meaningful since this direction is homogeneous (That is, spanwise vortices can occur randomly in x). Therefore, vortex centers are only categorized with respect to their wall-normal positions. Figure 2(a) presents the average number of negative spanwise vortices per velocity realization, N_n, at each Re_τ as a function of wall-normal position. The largest number of negative vortices is consistently found in the very-near-wall region ($y/h < 0.1$) at all three Re_τ, with N_n monotonically decreasing with wall-normal position. This behavior is consistent with the instantaneous velocity realization shown in Fig. 1 where a majority of the negative vortices appear below the outer edge of the log layer ($y/h < 0.2$). Such behavior also lends support to the idea that negative spanwise vortices, many of which are the heads of hairpin-like vortices, are generated very close to the wall, presumably due to the mean shear. Further, the decrease in N_n with y may indicate that the negative vortices grow away from the wall after their birth and increase in streamwise spacing as they advect downstream. This trend is consistent with the results of Christensen et al. (2004) who found that the average streamwise spacing of hairpin-like vortices in outer-layer vortex organization increases with wall-normal position. As such, fewer negative vortices, on average, would be expected to exist with increasing wall-normal position in any given PIV realization with a fixed streamwise field of view. Some portion of the decrease in N_n with y may also be associated with an increased probability of vortex merger/destruction as these vortices grow away from the wall. The recent work of Tomkins and Adrian (2003) details such merger/destruction scenarios.

In contrast to N_n, the average number of positive spanwise vortices per velocity realization, N_p,

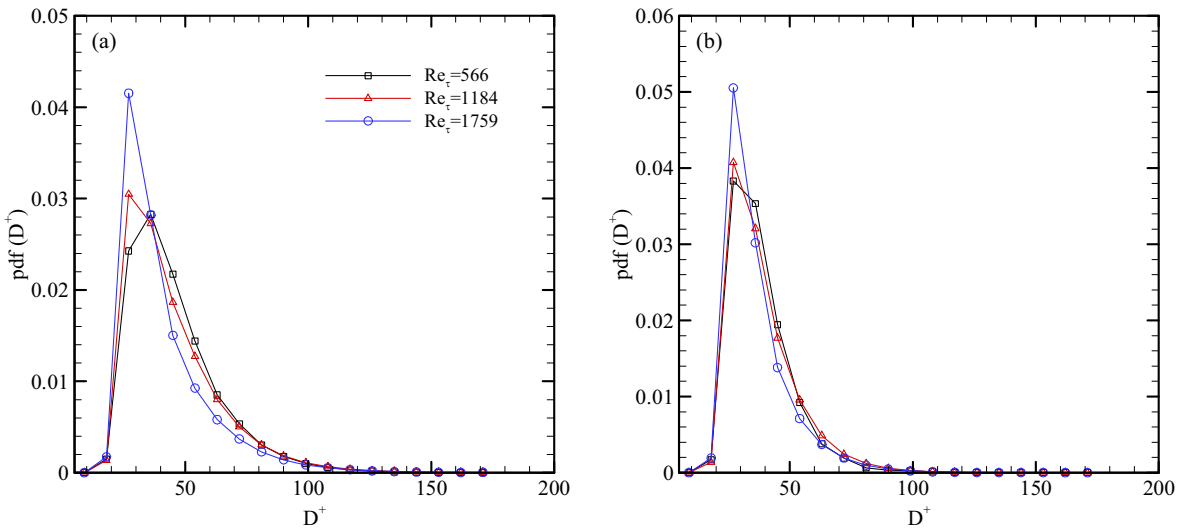

Fig. 3. Probability density functions of core diameters for (a) negative and (b) positive spanwise vortices.

(Fig. 2(b)) grows from nearly zero in the very-near-wall region to a strong peak near the outer edge of the log layer ($y/h \approx$ 0.15-0.2). Beyond the log layer, N_p decreases in a similar manner as N_n, but increases slightly between y/h = 0.75 and 1.0 (centerline). *Clearly, however, the majority of spanwise vortices in channel flow have clockwise rotation, particularly close to the wall where N_n can exceed N_p by nearly an order of magnitude.* The peak in N_p near y/h = 0.2 indicates that positive spanwise vortices may be generated by intense local shearing events in the log layer, in stark contrast to the notion that negative vortices are generated very close to the wall. One might explain the existence of these positive spanwise vortices by recalling that such vortices in the reference frame of the bottom wall of the channel are equivalently negative vortices in the reference frame of the top wall (since the y-coordinate is reflected about the centerline). Therefore, some percentage of the positive vortices might instead be associated with hairpin-like vortices generated at the top wall of the channel that have somehow traveled across the centerline and joined the flow along the bottom wall. However, recent measurements by the authors in a zero-pressure-gradient turbulent boundary layer, which does not suffer from an opposing wall, also show a peak in N_p at $y/\delta \approx$ 0.15-0.2, where δ is the boundary-layer thickness. Therefore, the majority positive spanwise vortices noted in the present study appear to be locally generated in the log layer.

Finally, the Reynolds-number trends in N_n and N_p can be partially explained by recalling that the size and spacing of these vortices scale with y_* (Christensen et al., 2004). The $1.3h$ streamwise field of view of the present PIV measurements grows with Re_τ when scaled by y_* ($1.3h = 736y_*$, $1539y_*$, and $2287y_*$ at Re_τ = 566, 1184 and 1759, respectively). Therefore, on average, more vortices can exist within this fixed field of view at higher Re_τ than at lower Re_τ. As such, one might expect roughly twice as many vortices to exist at Re_τ = 1184 than at Re_τ = 566 and roughly three-times as many spanwise vortices to exist at Re_τ = 1759 than at Re_τ = 566. The Reynolds-number trends of Fig. 2 are qualitatively consistent with this proposition.

4.3 Vortex Core Diameters

Probability density functions (pdf's) of vortex core diameters, D, for negative and positive spanwise vortices are presented in Figs. 3 (a) and (b), respectively. The core diameter of a given vortex is assessed from the vortex neighborhood information extracted during the vortex identification process. Specifically, the area occupied by a vortex is defined as the region for which $|\Lambda_{ci}| \geq \Lambda_{ci}^{rms}$ around each peak in $|\Lambda_{ci}|$. Also recall that any vortices for which fewer than three grid points meet this criterion in either spatial direction are discarded due to insufficient spatial resolution. Therefore, spanwise vortices less than approximately $18y_*$ in diameter, i.e., two grid spacings, are not considered in the present analysis. Most negative spanwise vortices are found to have diameters less than 60-75y_*. However, the pdf's of D for negative vortices have somewhat long tails, meaning that

larger negative vortices exist with diameters exceeding 90-100y_* at all three Re_τ. The widths of the pdf's narrow slightly with Re_τ, indicating that the average core diameter of negative spanwise vortices decreases slightly with Re_τ, even when scaled by y_*. In contrast, the pdf's of D for positive spanwise vortices are distinctly narrower than the pdf's for negative vortices, with few, positive vortices having core diameters exceeding 80y_*. As such, the average diameter of positive spanwise vortices is consistently smaller than the average diameter of negative vortices at all three Re_τ.

5. Summary

A methodology is presented for identification and visualization of small-scale vortices in wall-bounded turbulence. The methodology unambiguously identifies regions of rotation associated with small-scale vortices, even in regions of intense shear, and can discriminate between vortices with clockwise and counterclockwise rotation. Small-scale vortices extracted from large ensembles of high-resolution PIV fields in the streamwise–wall-normal plane of turbulent channel flow are then used to study their population trends and core diameters. The near-wall region is found to be densely populated by spanwise vortices with clockwise rotation (negative vorticity). This trend indicates that hairpin-like vortices are born very close to the wall and lift away from the wall as they advect downstream. In contrast, vortices with counterclockwise rotation (positive vorticity) are scarce in the near-wall region, but their numbers grow considerably within the logarithmic region. This growth in the log layer indicates that the generation of positive vortices may be associated with localized, intense turbulent events in the log layer. In addition, the core diameters of negative spanwise vortices tend to be larger than the core diameters of positive vortices, with few, if any, positive vortices exceeding 80y_* in diameter. Finally, the average core diameters of both positive and negative spanwise vortices appear to decrease slightly with Re_τ, even when scaled by y_*.

Acknowledgements

This work was financially supported by a Ralph Powe Junior Faculty Enhancement Award from Oak Ridge Associated Universities and by the University of Illinois. The experiments discussed herein were performed during the first author's tenure at The University of New Mexico.

References

Adrian, R. J., Christensen, K. T. and Liu, Z.-C., Analysis and interpretation of instantaneous turbulent velocity fields, Experiments in Fluids, 29 (2000a), 275-290.

Adrian, R. J., Meinhart, C. D. and Tomkins, C. D., Vortex organization in the outer region of the turbulent boundary layer, Journal of Fluid Mechanics, 422 (2000b), 1-54.

Chong, M. S., Perry, A. E. and Cantwell, B. J., A general classification of three-dimensional flow fields, Physics of Fluids A, 2 (1990), 765-777.

Christensen, K. T. and Adrian, R. J., Statistical evidence of hairpin vortex packets in wall turbulence, Journal of Fluid Mechanics, 431 (2001), 433-434.

Christensen, K. T., Soloff, S. M. and Adrian, R. J., PIV Sleuth – Integrated particle-image velocimetry interrogation/validation software, TAM Report, 943 (2000), University of Illinois at Urbana-Champaign, Urbana, Ill.

Christensen, K. T., Wu, Y., Adrian, R. J. and Lai, W., Statistical imprints of structure in wall turbulence, AIAA Paper 2004-1116 (2004).

Head, M. R. and Bandyopadhyay, P., New aspects of turbulent boundary-layer structure, Journal of Fluid Mechanics, 107 (1981), 297-338.

Jiménez, J., Wray, A. A., Saffman, P. G. and Rogallo, R. S., The structure of intense vorticity in isotropic turbulence, Journal of Fluid Mechanics, 255 (1993), 65-90.

Kim, K. C. and Adrian, R. J., Very large-scale motion in the outer layer, Physics of Fluids, 11 (1999), 417-422.

Kline, S. J. and Robinson, S. K., Quasi-coherent structures in the turbulent boundary layer. Part I: Status report on a community-wide summary of the data, Proceedings of Zaric Memorial Conference (Hemisphere), (1989), 200-217.

Marusic, I., On the role of large-scale structures in wall turbulence, Physics of Fluids, 13 (2001), 735-743.

Smith, C. R., A synthesized model of the near-wall behavior in turbulent boundary layers, Proceedings of the 8th Symposium on Turbulence, (1984), 299-325.

Theodorsen, T., Mechanisms of turbulence, Proceedings of the 2nd Midwestern Conference on Fluid Mechanics, (1952), 1-19.

Tomkins, C. D. and Adrian, R. J., Spanwise structure and scale growth in turbulent boundary layers, Journal of Fluid Mechanics, 490 (2003), 37-74.

Wu, Y., Spatial Characteristics of Outer-Layer Vortex Organization in Turbulent Channel Flow, (2004), M. S. Thesis, Department of Mechanical Engineering, The University of New Mexico, Albuquerque, NM.,

Zhou, J., Adrian, R. J., Balachandar, S. and Kendall, T. M., Mechanisms for generating coherent packets of hairpin vortices in channel flow, Journal of Fluid Mechanics, 387 (1999), 353-396.

Author Profile

Kenneth T. Christensen: He received an M.S. in Mechanical Engineering in 1996 from Caltech and a Ph.D. in Theoretical and Applied Mechanics in 2001 from the University of Illinois at Urbana-Champaign. He was an assistant professor of Mechanical Engineering at the University of New Mexico prior to his current position as an assistant professor in the Theoretical and Applied Mechanics Department at the University of Illinois at Urbana-Champaign. His research interests include turbulence, microscale flows, cardiovascular fluid dynamics, multiphase flows and advanced experimental methods.

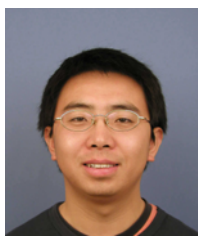

Yanhua Wu: He received an M.S. in Mechanical Engineering in 2004 from the University of New Mexico and is currently a Ph.D. student in the Theoretical and Applied Mechanics Department at the University of Illinois at Urbana-Champaign. His research interests include the effect of roughness and straining on the structure of wall turbulence and advanced experimental methods.